ACS OMEGA

http://pubs.acs.org/journal/acsodf

Article

Sepiolite Nanocarriers as a Matrix for Controlled Thermal Energy Storage

Xiaolei Zhu, Vladimir Vinokurov, Dmitry Kopitsyn, and Dmitry G. Shchukin*

Cite This: *ACS Omega* 2021, 6, 25828−25834

Read Online

ACCESS | Metrics & More | Article Recommendations | Supporting Information

ABSTRACT: Applying the eutectic hydrated salt (EHS) mixture of $Na_2HPO_4{\cdot}12H_2O$ and $Na_2SO_4{\cdot}10H_2O$ in a 1:1 weight ratio as a phase-change material and natural sepiolite nanocarriers as a matrix, the form-stable phase-change composite EHS@sepiolite was fabricated by vacuum impregnation. Due to the high porosity of sepiolite and its nanofibrous structure with internal channels, the effective loading of the phase-change material reached as high as 88 wt %. The melting temperature of the composite was 38.1 °C and its melting enthalpy was 185 J $g^{-1.}$ The crystallinity of the hydrated salt mixture was retained after loading into the sepiolite matrix. The composite demonstrated high stability over 50 heat uptake/release cycles maintaining its melting temperature and melting enthalpy the same. The combination of natural sepiolite nanocarriers and crystallohydrates is a cheap and efficient nanoscale energy storage system with high potential for practical applications and upscaling because of their natural abundance.

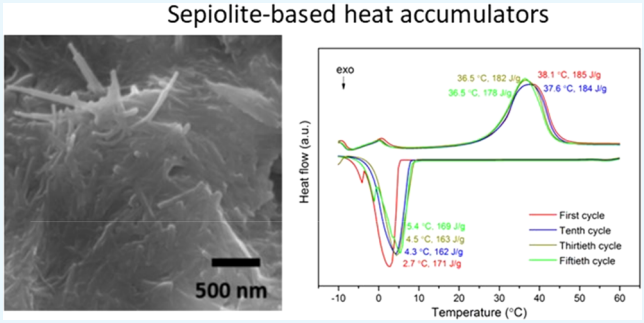

INTRODUCTION

To address the serious global problem of changing energy supply due to the limited resources of traditional fossil fuels and environmental pollution during their utilization,[1] many countries, funding agencies, and researchers are motivated to improve the efficiency of energy use, especially for thermal energy which consumes one-third of the worldwide energy supply.[2] Phase-change materials (PCMs) use the principle of latent heat storage at a constant phase-change temperature and have high energy storage density.[3−5] PCMs demonstrated high efficiency to facilitate the application of thermal solar energy[6] and use of waste heat.[7] Hydrated salts (crystallohydrates) as a main group of inorganic PCMs exhibit (i) low costs, (ii) environmental friendliness, (iii) nonflammability, (iv) high phase-change enthalpy, and (v) good thermal conductivity.[8−10] Despite all of these advantages, hydrated salts are still underrepresented in PCM applications. One major drawback is the leakage of crystallohydrate PCM water during its transformation from solid to liquid form and back.[11] The other non-negligible problems are the internal phase separation by incongruent melting, corrosiveness, and supercooling due to the low nucleation rate.[12,13]

The fabrication of form-stable PCM composites (FSPCMs) can be an effective way to improve energy storage performances of phase-change materials. There are several papers describing the formation of organic PCM composites, which demonstrate increased thermal performance of the incorporated organic PCMs, especially into hallysite nanotubes.[14−16] Halloysite nanotubes were also demonstrated as a prospective tubular host in biomedical applications[17,18] and environmental decontamination.[19]

FSPCMs based on crystallohydrate salt eutectics have been demonstrated using organic hosts stabilized by carbon nanocomposites: carbon nanofiber-expanded graphite,[20] MWCNT-modified hydrate salt/poly-(acrylate sodium) copolymer hydrogels,[21] and acrylic resin with incorporated graphene oxide.[22] Additional information about FSPCMs with organic hosts can be found in a review paper.[23]

As a natural magnesium silicate mineral material, sepiolite has low cost and is highly abundant. It has a high specific surface area due to its long fibrous morphology and internal channel structure. Other important merits of sepiolite include its high thermal stability, good mechanical properties, chemical resistance, and flame retardancy.[24] As a result, sepiolite is a widely applied raw material in industry,[25] for example, in heterogeneous catalysts[26] and adsorbents.[27,28] The application of sepiolite for thermal energy storage was already reported for loading with organic phase-change materials.[29−34] However, no studies of hydrated salts as PCMs loaded into the sepiolite matrix were found by us despite the unique sepiolite nanosized

Received: August 14, 2021
Published: September 20, 2021

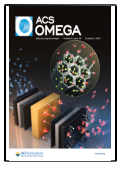

internal channels and hydrophilic surface, which can stabilize inorganic PCM during heat uptake/release cycles.

In this work, sepiolite was chosen as the matrix material to incorporate an inorganic EHS (1 disodium hydrogen phosphate dodecahydrate (DHPD):-1 sodium sulfate decahydrate (SDH)) by vacuum impregnation[35] to form EHS@sepiolite composites with various EHS loadings. The morphology, chemical bonding, and crystallinity of the composites were investigated and compared with the pure EHS and sepiolite. The thermal energy storage and the cycling stability were characterized by dynamic scanning calorimetry (DSC). The relationship between the phase-change behavior of the EHS@sepiolite composite, structure, and influence of sepiolite as the host matrix on thermal properties was discussed.

RESULTS AND DISCUSSION

Morphology and Pore Structure of Pure Sepiolite. Scanning electron microscopy (SEM) images of sepiolite nanocarriers are shown in Figure 1. Sepiolite has a long tubular

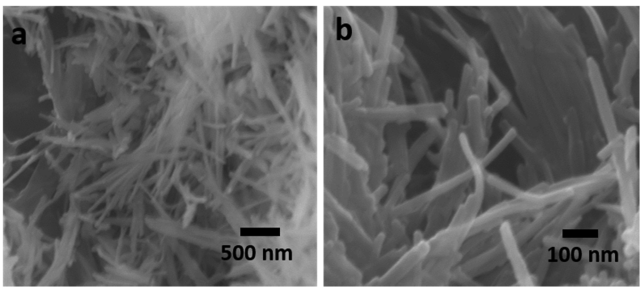

Figure 1. SEM images of sepiolite nanocarriers with a magnification of (a) 20 000 and (b) 40 000.

morphology with a length from 1 to 5 μm and an average diameter of 30 nm. Nanocarriers tend to aggregate and tangle with each other forming tubular networks. The aggregation could result from the hydrogen bonding between Si−OH groups on the external surface of nanocarriers and a small amount of adhered water inside forming a network structure.[36]

The N_2 adsorption−desorption isotherms of sepiolite are shown in Figure 2. The isotherms are of type IV, demonstrating a mesoporous structure of the sepiolite network. The hysteresis loop is of H1 type, indicating a cylindrical pore geometry with a fairly uniform pore size. According to the Brunauer−Emmett−Teller (BET) calculation, the sepiolite network has a very high pore volume of 0.64

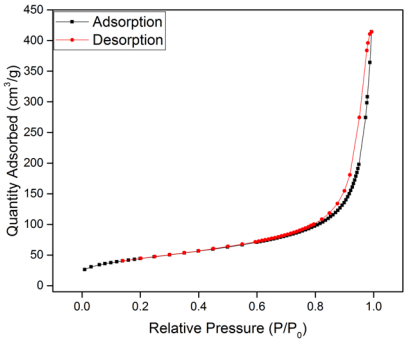

Figure 2. N_2 adsorption−desorption isotherms of sepiolite.

$cm^3\ g^{-1}$ and specific surface area of 156.82 $m^2\ g^{-1}$. The large pore volume of the sepiolite network further resulted in high loading volumes of PCM.

The pore size distribution from the BJH analysis is shown in Figure 3. The pore size at 24 nm gives the highest pore

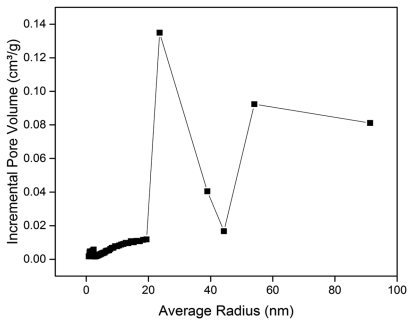

Figure 3. Pore size distribution of the sepiolite network.

volume, which could be attributed to the inner channels of sepiolite. The pores at 54 and 91 nm, which are bigger than the average diameter of sepiolite nanocarriers, resulted from the inner voids of the intermeshed sepiolite nanocarriers (network).

Influence of EHS@Sepiolite Loading on Heat Storage Properties. The DSC melting curves of EHS@sepiolite composites with EHS loadings ranging from 50 to 90 wt % are displayed in Figure 4. The corresponding melting

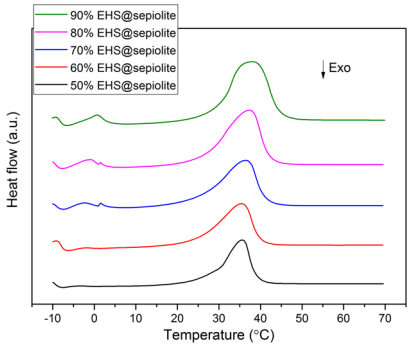

Figure 4. DSC melting curves of EHS@sepiolite composites with EHS loadings from 50 to 90 wt %.

temperature, melting enthalpy, and the calculated effective loading are listed in Table 1. EHS@sepiolite composites showed no water loss and formation of new crystallohydrate phases during melting and heat uptake. The absence of water leakage in the EHS@sepiolite composite was visually confirmed on the optical photos of pure EHS and EHS@

Table 1. DSC Data for Melting Curves of EHS@Sepiolite Composites with Various EHS Loadings

EHS mass ratio in EHS@sepiolite	melting temperature (°C)	melting enthalpy (J g^{-1})	effective loading (wt %)
50%	35.5	102	48
60%	35.7	120	57
70%	36.4	140	66
80%	37.3	158	75
90%	38.1	185	88

https://doi.org/10.1021/acsomega.1c04392
ACS Omega 2021, 6, 25828−25834

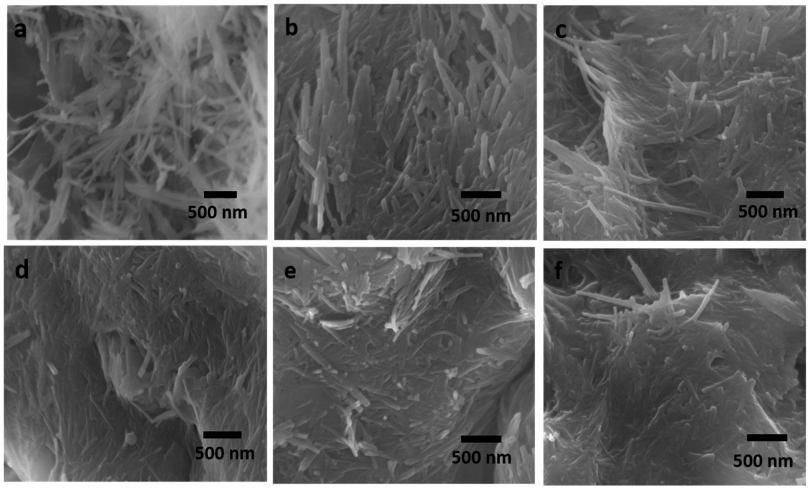

Figure 5. SEM images of (a) sepiolite and (b) 50 wt %, (c) 60 wt %, (d) 70 wt %, (e) 80 wt %, and (f) 90 wt % EHS@sepiolite composites.

sepiolite composites with and without a mechanical load (see Figures S1 and S2). The melting peaks of the composites are uniform, all of them between 35.5 and 38.5 °C. The peak shifts to a slightly higher temperature as the loading of EHS in the composite increases. The 50 wt % EHS@sepiolite composite exhibits the melting point at 35.5 °C, while the 90 wt % composite melts at 38.1 °C, which is similar to the melting point of pure EHS at 38.5 °C (see Figure 11a).

The shape of the melting curves turns broader as the loading increases. This suggests that some EHS is not confined in the nanochannels or network of sepiolite nanocarriers with a higher loading. The melting enthalpy of the composite grows with the mass ratio of EHS at a consistent rate of about 2 J g^{-1} wt $\%^{-1}$. The loading efficiency of each composite is approximately the same as the theoretical loading ratio of EHS with less than 5 wt % loss.

The SEM images of sepiolite and EHS@sepiolite composites with various EHS loadings are presented in Figure 5. While the unloaded sepiolite nanocarriers are loosely distributed, the composites show compactness forming the network with EHS. The nanocarriers are closely arranged next to each other at 50 wt % EHS@sepiolite composite loading. The individual nanocarriers are still distinguishable with small voids between them or inside their bundles. No EHS material was observed outside the sepiolite network confirming that salt hydrates are entrapped in the sepiolite matrix at 50 wt % EHS loading. The 60 wt % EHS@sepiolite composite displays a more compact structure. The nanocarriers are adhered to each other due to the hydrogen bonding between the absorbed water and −OH groups on their surface.[33,34] No obvious leakage of impregnated material was found on the surface of the composite network. The 70, 80, and 90 wt % EHS@sepiolite composites showed similar morphology to that for the 60 wt % EHS@sepiolite composite. Nanocarriers are tightly assembled forming a sheet-like material, and voids are hardly observed between them. No EHS was found outside the composite network.

The change of melting enthalpies of the EHS@sepiolite composite with 50, 60, 70, 80, and 90 wt % loadings at different thermal cycling numbers is illustrated in Figure 6. DSC data of the heat uptake/release cycles are listed in Tables S1−S5. The decrements of the melting enthalpy after 50 cycles are 2.3, 6.6, 0.5, 2.4, and 3.6% for the 50, 60, 70, 80, and 90 wt % composites, respectively. As the loading of EHS increased,

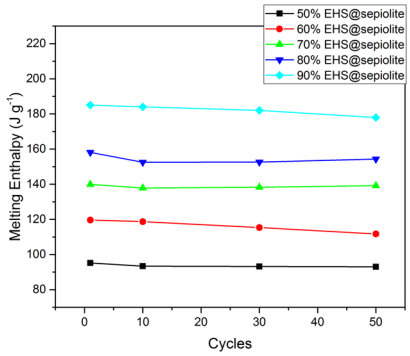

Figure 6. Melting enthalpies of EHS@sepiolite composites with various EHS loadings vs numbers of heat uptake cycles.

no evident reduction of melting enthalpy with growing cycling numbers was observed. The melting enthalpy of the 90% EHS@sepiolite composite reduced only by 7 J g^{-1} after 50 cycles. The 90 wt % composite sample was used for further characterizations in this work because of the highest EHS loading, heat capacity, and good cycling stability.

Characterization of the EHS@Sepiolite Composite with 90 wt % EHS Loading. The transmission electron microscopy (TEM) images of sepiolite and the 90 wt % EHS@sepiolite composite are shown in Figure 7. Sepiolite fibers (Figure 7A) are thin with an average diameter of 30 nm, and a length from 1 to 5 μm, which is consistent with the observation from SEM images (Figure 1). Parallel hollow channels can be observed in TEM image of sepiolite fibers (Figure 7A2). These nanochannels are formed by continuous SiO_2 tetrahedrons and discontinuous MgO octahedrons.[37] TEM images of EHS-filled sepiolite nanocarriers from the 90 wt % EHS@sepiolite composite (Figure 7B) showed different structures compared with pure sepiolite nanocarriers with EHS as dark irregular blocks of ca. 5 nm size intercalated into individual sepiolite nanocarriers (Figure 7B1). Single EHS nanoparticles as dark dots were also detected inside the sepiolite tube (Figure 7B2), indicating the filling of nanochannels of sepiolite with EHS. This confirms that EHS is not only entrapped within the sepiolite network but also can be hosted inside sepiolite nanochannels.

The energy-dispersive X-ray spectroscopy (EDS) spectra of sepiolite and the 90 wt % EHS@sepiolite composite are shown

https://doi.org/10.1021/acsomega.1c04392
ACS Omega 2021, 6, 25828−25834

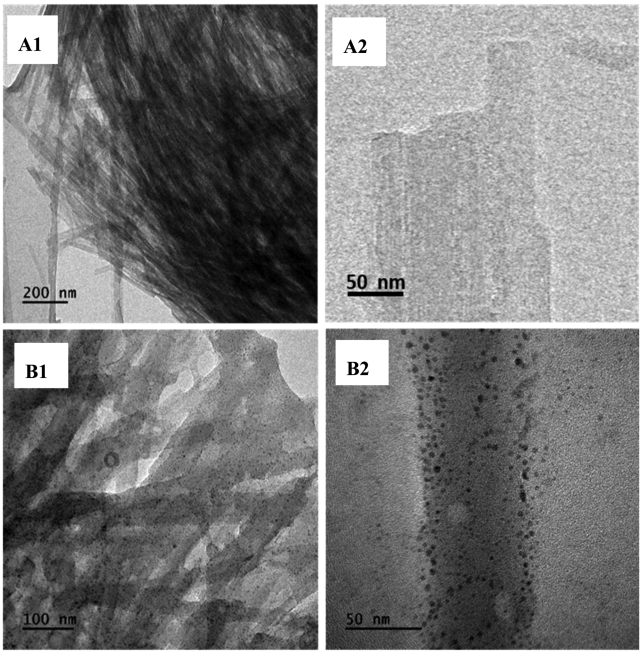

Figure 7. TEM images of (A) pure sepiolite and (B) the 90 wt % EHS@sepiolite composite.

in Figure 8. Strong peaks of O, Mg, and Si shown in EDS spectra are related to sepiolite MgO and SiO_2 nanosheets

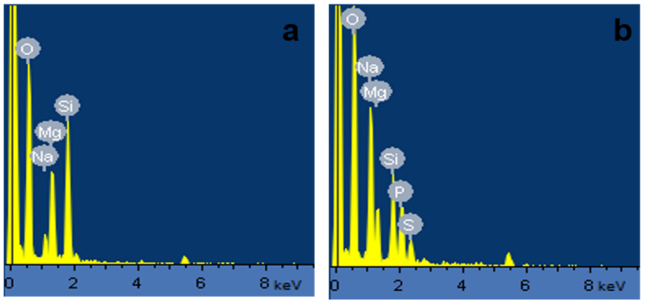

Figure 8. EDS of (a) pure sepiolite and (b) the 90 wt % EHS@sepiolite composite.

(Figure 8a). The small peak of Na resulted from the presence of Na^+ inside sepiolite channels. In the composite, new peaks of P and S and increased intensity of Na and O peaks were observed confirming the presence of EHS.

The Fourier transform infrared (FTIR) spectrum of the 90 wt % EHS@sepiolite composite and spectra of EHS and pure sepiolite are shown in Figure 9. Sepiolite exhibits characteristic peaks at 1011 and 971 cm^{-1} from the stretching vibrations of Si−O. The peaks at 464 and 427 cm^{-1} are from the deformation vibrations of Si−O−Mg. EHS has peaks at 1077 and 985 cm^{-1} due to the vibration of P−O bonding. In the composite, the peaks from sepiolite and from EHS at around 1000 cm^{-1} merge together and generate a broad peak at 1075 cm^{-1} with a strong shoulder at 988 cm^{-1}. A relatively broad peak at 468 cm^{-1} in the composite is considered as a combination of Si−O−Mg vibration peaks and the peak at 521 cm^{-1} in the EHS spectrum. The strong broad peak at 3341 cm^{-1} from the O−H stretching of hydrated water and the sharp peak at 1669 cm^{-1} from the P−OH stretching vibration were observed without shift in both EHS and EHS@sepiolite

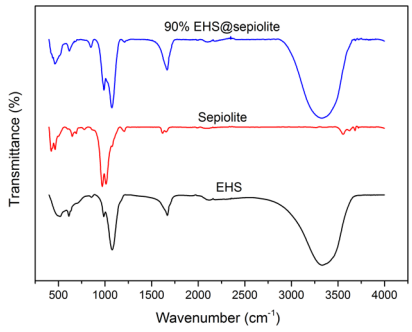

Figure 9. FTIR spectra of EHS, pure sepiolite, and 90 wt % EHS@sepiolite composite.

composites. No new peaks except from sepiolite and EHS were found in the EHS@sepiolite composite, indicating no covalent bonding is formed between the EHS and sepiolite.

The crystal structure of the 90 wt % EHS@sepiolite composite was characterized by the X-ray diffraction (XRD) pattern as shown in Figure 10. The diffraction peaks from the

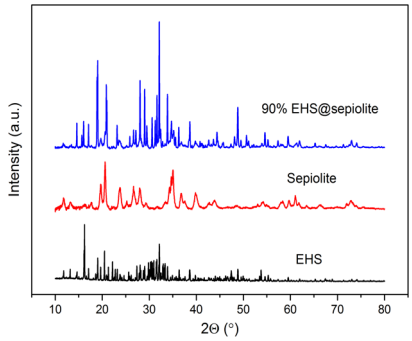

Figure 10. XRD patterns of EHS, sepiolite, and the 90 wt % EHS@sepiolite composite.

sepiolite including those at 2Θ values of at 19.6, 20.6, 23.8, 35.1, 36.8, 39.8, and 73.0° were also observed in the XRD pattern of the 90 wt % EHS@sepiolite composite, indicating the crystal structure of the sepiolite remained in the EHS@sepiolite composite. However, the typical diffraction peaks from EHS at 2Θ values of 19.0, 23.2, 29, 33.9, 38.7, and 48.8° were also observed in the composite, also demonstrating the intact crystal structure of the embedded EHS.

The DSC curves of pure EHS and the 90 wt % EHS@sepiolite composite for 50 thermal cycles are shown in Figure 11a,b. The detailed phase-change data from the cycling curves are summarized in Table S5 for the 90 wt % EHS@sepiolite and Table S6 for EHS. The 90 wt % EHS@sepiolite composite has a melting point of 38.1 °C and a melting enthalpy of 185 J g^{-1} corresponding to the 88 wt % loading efficiency of EHS. The phase-change behavior of the composite is stable during more than 50 heat uptake/release cycles with a small shift of the crystallization temperature by 2.7 °C with the crystallization and melting enthalpies remaining the same. No phase separation was observed in the melting curves, and the freezing behavior was consistent. On the contrary, pure EHS lost 70% of its energy storage enthalpy and demonstrated crystallohydrate phase separation at the 50th heat uptake/release cycle.

Compared with the phase-change behavior of pure EHS for 50 cycles in Figure 11a, the EHS@sepiolite composite shows obviously better thermal cycling resistance. This results from

https://doi.org/10.1021/acsomega.1c04392
ACS Omega 2021, 6, 25828−25834

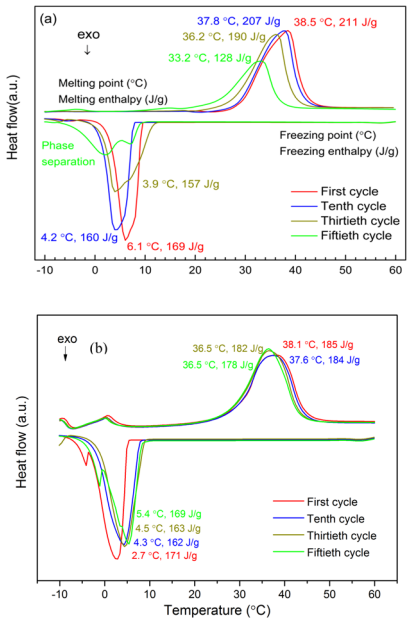

Figure 11. Thermal cycling tests of (a) pure EHS and (b) the 90 wt % EHS@sepiolite composite for 50 cycles.

the special composition and structure of sepiolite. One part of hydrated salts is absorbed inside the nanochannels of sepiolite fibers. The capillary effect and the hydrogen bonding hold the hydrated salts stable in nanochannels after melting and cooling during the heat uptake/release. In the presence of water, sepiolite fibers tend to intermesh densely with each other to form a sepiolite network. The highest part of the EHS is kept in the small voids inside the network stabilizing its heat uptake and release parameters. The hydrogen bonding between Mg−OH of sepiolite and P−O from EHS prevents leakage of EHS outside the network. Furthermore, the absorbed water in sepiolite nanochannels prevents loss of hydrated water during the heat uptake and release.

CONCLUSIONS

Sepiolite natural nanocarriers were applied as matrix materials to host eutectic hydrated salts (EHSs) with 50 wt % $Na_2HPO_4 \cdot 12H_2O$ and 50 wt % $Na_2SO_4 \cdot 10H_2O$ to form EHS@sepiolite composites for thermal energy storage. Sepiolite has an elongated nanotubular morphology with an average diameter of 30 nm and a nanocarrier length ranging from 1 to 5 μm. The unique structure of sepiolite determines its high specific surface area of 156.82 $m^2 \cdot g^{-1}$ and large pore volume of 0.64 $cm^3 \cdot g^{-1}$, which enables its high PCM loading capacity of up to 90 wt % EHS inside the sepiolite network. Furthermore, water molecules inside sepiolite nanochannels and presence of Si−OH groups on the surface of nanocarriers function as active hydrogen-bonding sites to interact with hydrated salts. The EHS@sepiolite composite with 90 wt % effective loading was successfully fabricated and demonstrated the highest loading capacity and cycling performance among investigated composites with a melting enthalpy of 185 J g^{-1} and melting temperature of 38.1 °C, which was stable over 50 heat uptake/release cycles. The X-ray characterization indicated an unchanged crystal structure of both sepiolite and EHS in the composite. No covalent bonding was observed between crystallohydrates and the sepiolite matrix.

Considering the low cost and the abundant natural reserves of sepiolite and crystallohydrates, the simple fabrication procedure, the high loading efficiency, and the good cycling stability, the fabricated EHS@sepiolite composites have shown large potential for thermal energy storage applications for the use of the so-called waste heat (heat with temperatures below 180 °C), which usually dissipates into the environment, for temperature control in domestic applications.

EXPERIMENTAL SECTION

Materials. Disodium hydrogen phosphate dodecahydrate ($Na_2HPO_4 \cdot 12H_2O$, DHPD, purity >99%) and sodium sulfate decahydrate ($Na_2SO_4 \cdot 10H_2O$, SDH, purity >99%) were supplied by Sigma-Aldrich, Germany. Eutectic hydrated salts (EHSs) with 50 wt % SDH:50 wt % DHPD composite was applied as the PCM material for sepiolite loading. Sepiolite (nanoclay) was purchased from Sigma-Aldrich, U.K. It was dried at 120 °C for 12 h before use. All other materials were used as received without further purification. Milli-Q water was applied in all experiments.

Characterization Methods. The specific surface area of the sepiolite was measured by N_2 adsorption isotherms at 77 K using a 3Flex Version 5.00 from Micrometritics Instruments. The samples were degassed at 250 °C for 2 h before measurements. The pore size distribution was analyzed by the Barrett−Joyner−Halenda (BJH) method.

The morphology of sepiolite and the prepared composites was characterized by scanning electron microscopy (SEM, JSM-7001F, JEOL Japan). The powder samples were coated with a 100 nm chromium layer under vacuum before measurements. The inner structure of sepiolite and composites was evaluated by transmission electron microscopy (TEM, STEM-2100F, JEOL Japan) at 200 kV.

Fourier transform infrared spectroscopy (FTIR, Bruker with TENSOR II instrument, Germany) was used to investigate the chemical composition of the composites in the 400−4000 cm^{-1} wavenumber range. X-ray diffraction (XRD, Bruker diffractometer with Cu Kα radiation) was applied to analyze the crystalline structure of samples. The scans were recorded from 2Θ of 10 to 80° within 1 h.

The phase-change properties and cycling stability were analyzed using a differential scanning calorimeter (DSC 214 NETSCH, Germany). Samples, each weighing 10−15 mg, were sealed in an aluminum pan for measurement. The analysis was performed from −20 to 70 °C under nitrogen. The heating and cooling rate was 10 °C min^{-1}.

Synthetic Methods. To fabricate EHS@sepiolite composites, first EHS water solutions were prepared by dissolving 7 g of EHS in 3 mL of water at 40 °C. Then, 7, 4.67, 3, 1.75, 0.78, and 0.37 g of sepiolite was added to each solution to form EHS/sepiolite dispersions with weight ratios of EHS of 50, 60, 70, 80, 90 and 95%. The dispersions were sonicated (VWR Ultrasonic Cleaner USC 500TH, output 100 W) at 40 °C for 30 min and then kept at room temperature for 10 min. The 95% dispersion was inhomogeneous and was not further investigated, while other dispersions resulted in light gray homogeneous suspensions. Then, all of the samples were put under vacuum at 40 °C for 10 min and exposed to air at room temperature for 10 min. This process was repeated twice to achieve saturation of the sepiolite loading. The density and viscosity of the mixtures decreased as the mass ratio of EHS increased. Samples with 50−90% of EHS loading were further cooled at 4 °C for 30 min and dried in a desiccator at room

https://doi.org/10.1021/acsomega.1c04392
ACS Omega 2021, 6, 25828−25834

temperature for 2 days until their weight became constant. A light gray powder was obtained as the end product for all samples.

■ ASSOCIATED CONTENT

Supporting Information

The Supporting Information is available free of charge at https://pubs.acs.org/doi/10.1021/acsomega.1c04392.

(i) Optical photos of the pure EHS mixture and 90 wt % EHS@sepiolite composite before and after heating to 50 °C both with and without mechanical pressure and (ii) thetabulated DSC data of 50, 60, 70, 80, and 90 wt % EHS@sepiolite composite for 50 heating/cooling cycles and for pure EHS (PDF)

■ AUTHOR INFORMATION

Corresponding Author

Dmitry G. Shchukin − *Stephenson Institute for Renewable Energy, University of Liverpool, Liverpool L69 7ZF, United Kingdom; Gubkin University, Moscow 119991, Russia;* orcid.org/0000-0002-2936-804X; Email: d.shchukin@liverpool.ac.uk

Authors

Xiaolei Zhu − *Stephenson Institute for Renewable Energy, University of Liverpool, Liverpool L69 7ZF, United Kingdom*

Vladimir Vinokurov − *Gubkin University, Moscow 119991, Russia*

Dmitry Kopitsyn − *Gubkin University, Moscow 119991, Russia*

Complete contact information is available at: https://pubs.acs.org/10.1021/acsomega.1c04392

Notes

The authors declare no competing financial interest.

■ ACKNOWLEDGMENTS

This work was supported by ERC Grant ENERCAPSULE (#647969), RSC Grant IEC\NSFC\181714, and RSF Grant (#19-79-30091).

■ REFERENCES

(1) Gielen, D.; Boshell, F.; Saygin, D.; Bazilian, M. D.; Wagner, N.; Gorini, R. The Role of Renewable Energy in the Global Energy Transformation. *Energy Strategy Rev.* **2019**, *24*, 38−50.

(2) Borri, E.; Zsembinszki, G.; Gabriel, L. F. Recent Developments of Thermal Energy Storage Applications in the Built Environment: A Bibliometric Analysis and Systematic Review. *Appl. Therm. Eng.* **2021**, *189*, No. 116666.

(3) Khan, Z.; Khan, Z.; Ghafour, A. A Review of Performance Enhancement of PCM Based Latent Heat Storage System within the Context of Materials, Thermal Stability and Cmpatibility. *Energy Convers. Manage.* **2016**, *115*, 132−158.

(4) Shchukina, E.; Graham, M.; Zheng, Z.; Shchukin, D. Nanoencapsulation of Phase Change Materials for Advanced Thermal Energy Storage Systems. *Chem. Soc. Rev.* **2018**, *47*, 4156−4175.

(5) Shchukina, E.; Shchukin, D. Nanocontainer-Based Active Systems: From Self-Healing Coatings to Thermal Energy Storage. *Langmuir* **2019**, *35*, 8603−8611.

(6) Zhou, Z.; Zhang, Z.; Zuo, J.; Huang, K.; Zhang, L. Phase Change Materials for Solar Thermal Energy Storage in Residential Buildings in Cold Climate. *Renewable Sustainable Energy Rev.* **2015**, *48*, 692−703.

(7) Miró, L.; Gasia, J.; Cabeza, L. F. Thermal Energy Storage (TES) for Industrial Waste Heat (IWH) Recovery: A Review. *Appl. Energy* **2016**, *179*, 284−301.

(8) Graham, M.; Shchukina, E.; Felix de Castro, P.; Shchukin, D. Nanocapsules Containing Salt Hydrate Phase Change Materials for Thermal Energy Storage. *J. Mater. Chem. A* **2016**, *4*, 16906−16912.

(9) Graham, M.; Coca-Clemente, J.; Shchukina, E.; Shchukin, D. Nanoencapsulated Crystallohydrate Mixtures for Advanced Thermal Energy Storage. *J. Mater. Chem. A* **2017**, *5*, 13683−13691.

(10) Kenisarin, M.; Mahkamov, K. Salt Hydrates as Latent Heat Storage Materials: Thermophysical Properties and Costs. *Sol. Energy Mater. Sol. Cells* **2016**, *145*, 255−286.

(11) Drissi, S.; Ling, T. C.; Mo, K. H. Development of Leak-Free Phase Change Material Aggregates. *Constr. Build. Mater.* **2020**, *230*, No. 117029.

(12) Tian, G.; Han, G.; Wang, F.; Liang, J. Sepiolite Nanomaterials: Structure, Properties and Functional Applications. In *Nanomaterials from Clay Minerals*; Wang, A.; Wang, W., Eds.; Elsevier, 2019; pp 135−201.

(13) Cabeza, L. F.; Illa, J.; Roca, J.; Badia, F.; Mehling, H.; Hiebler, S.; Ziegler, F. Immersion Corrosion Tests on Metal-Salt Hydrate Pairs Used for Latent Heat Storage in the 32 to 36 °C Temperature Range. *Mater. Corros.* **2001**, *52*, 140−146.

(14) Porisini, F. C. Salt Hydrates Used for Latent Heat Storage: Corrosion of Metals and Reliability of Thermal Performance. *Sol. Energy* **1988**, *41*, 193−197.

(15) Zhao, Y.; Thapa, S.; Weiss, L.; Lvov, Y. Phase Change Heat Insulation Based on Wax-Clay Nanotube Composites. *Adv. Eng. Mater.* **2014**, *16*, 1391−1399.

(16) Chai, S. Y.; Sun, K. Y.; Zhao, D. H.; Kou, Y.; Shi, Q. Form-Stable Erythritol/HDPE Composite Phase Change Material with Flexibility, Tailorability and High Transition Enthalpy. *ACS Appl. Polym. Mater.* **2020**, *2*, 4464−4471.

(17) Liu, M.; Fakhrullin, R.; Novikov, A.; Panchal, A.; Lvov, Y. Tubule Nanoclay-Organic Heterostructures for Biomedical Applications. *Macromol. Biosci.* **2019**, *19*, No. 1800419.

(18) Cavallaro, G.; Lazzara, G.; Fakhrullin, R. Mesoporous inorganic nanoscale particles for drug adsorption and controlled release. *Ther. Delivery* **2018**, *9*, 287−301.

(19) Cavallaro, G.; Lazzara, G.; Rozhina, E.; Konnova, S.; Kryuchkova, M.; Khaertdinov, N.; Fakhrullin, R. Organic-Nanoclay Composite Materials as Removal Agents for Environmental Decontamination. *RSC Adv.* **2019**, *9*, 40553.

(20) Yu, K.; Jin, B.; Liu, Y.; Li, L. Enhanced Thermal Conductivity of Form-Stable Phase Change Materials Using Carbon Nanofiber-Expanded Graphite Hybrid Structure. *Mater. Res. Express* **2019**, *6*, No. 125503.

(21) Liu, Y.; Yu, K.; Gao, X.; Ren, M.; Jia, M.; Yang, Y. Enhanced Thermal Properties of Hydrate Salt/Poly (Acrylate Sodium) Copolymer Hydrogel as Form-Stable Phase Change Material via Incorporation of Hydroxyl Carbon Nanotubes. *Sol. Energy Mater. Sol. Cells* **2020**, *208*, No. 110387.

(22) Liu, Y.; Yu, K.; Xie, M.; Lu, S.; Yang, Y.; Wang, H.; Jia, H. Hydrate Salt/Self-Curing Acrylic Resin Form-Stable Phase Change Materials with Enhanced Surface Stability and Thermal Properties via the Incorporation of Graphene Oxide. *Int. J. Energy Res.* **2020**, *44*, 5791−5805.

(23) Yu, K.; Liu, Y.; Yang, Y. Review on Form-Stable Inorganic Hydrated Salt Phase Change Materials: Preparation, Characterization and Effect on the Thermophysical Properties. *Appl. Energy* **2021**, *292*, No. 116845.

(24) Kotal, M.; Bhowmick, A. K. Polymer Nanocomposites from Modified Clays: Recent Advances and Challenges. *Prog. Polym. Sci.* **2015**, *51*, 127−187.

(25) Galan, E. Properties and Applications of Palygorskite-Sepiolite Clays. *Clay Miner.* **1996**, *31*, 443−453.

(26) Ma, Y.; Zhang, G. Sepiolite Nanofiber-Supported Platinum Nanoparticle Catalysts toward the Catalytic Oxidation of Form-

aldehyde at Ambient Temperature: Efficient and Stable Performance and Mechanism. *Chem. Eng. J.* **2016**, *288*, 70−78.
(27) Akkari, M.; Aranda, P.; Belver, C.; Bedia, J.; Ben Haj Amara, E.; Ruiz-Hitzky, E. Reprint of ZnO/Sepiolite Heterostructured Materials for Solar Photocatalytic Degradation of Pharmaceuticals in Wastewater. *Appl. Clay Sci.* **2018**, *160*, 3−8.
(28) Marrakchi, F.; Khanday, W. A.; Asif, M.; Hameed, B. H. Cross-Linked Chitosan/Sepiolite Composite for the Adsorption of Methylene Blue and Reactive Orange. *Int. J. Biol. Macromol.* **2016**, *93*, 1231−1239.
(29) Santos, S. C. R.; Boaventura, R. A. R. Adsorption of Cationic and Anionic Azo Dyes on Sepiolite Clay: Equilibrium and Kinetic Studies in Batch Mode. *J. Environ. Chem. Eng.* **2016**, *4*, 1473−1483.
(30) Voronin, D. V.; Ivanov, E.; Gushchukin, P.; Fakhrulin, R.; Vinokurov, V. Clay Composites for Thermal Energy Storage: A Review. *Molecules* **2020**, *25*, No. 1504.
(31) Vassilev, S. V.; Braekman-Danheux, C.; Laurent, P. Characterization of Refuse-Derived Char from Municipal Solid Waste: 1. Phase-Mineral and Chemical Composition. *Fuel Process. Technol.* **1999**, *59*, 95−134.
(32) Liang, J. S.; Wu, Z. Z.; Liang, G. C.; Li, G. S.; Yin, H.; Wang, J.; Liang, X. H. Preparation of the Composite Materials with Dodecanol and Sepiolite for Self-Operating Temperature. *Rare Met. Mater. Eng.* **2004**, *33*, 110−113.
(33) Cannings, F. R. Infrared Study of Hydroxyl Groups on Sepiolite. *J. Phys. Chem. A* **1968**, *72*, 1072−1074.
(34) Prost, R. Infrared Study of the Interactions between the Different Kinds of Water Molecules Present in Sepiolite. *Spectrochim. Acta, Part A* **1975**, *31*, 1497−1499.
(35) Zhu, X.; Shchukin, D. Crystallohydrate Loaded Halloysite Nanocontainers for Thermal Energy Storage. *Adv. Eng. Mater.* **2018**, *20*, No. 1800618.
(36) Serna, C.; Ahlrichs, J. L.; Serratosa, J. M. Folding in Sepiolite Crystals. *Clays Clay Miner.* **1975**, *23*, 452−457.
(37) Post, J. E.; Bish, D. L.; Heaney, P. J. Synchrotron Powder X-ray Diffraction Study of the Structure and Dehydration Behavior of Sepiolite. *Am. Mineral.* **2007**, *92*, 91−97.

https://doi.org/10.1021/acsomega.1c04392
ACS Omega 2021, 6, 25828−25834